Supporting Information

Ultra-strong, Nonfreezing, and Flexible Strain Sensor Enabled by Biomass-based Hydrogels through Triple Dynamic Bond Design

Haocheng Fu, Bin Wang *, Jinpeng Li, Daxian Cao, Wei Zhang*, Jun Xu, Jun Li, Jinsong Zeng, Wenhua Gao, Kefu Chen

This word file includes the following parts:

Experimental Section

Supporting Figure S1 to S20

Supporting Tables S1 to S3

Other Supplementary Materials include the following:

Supporting Video S1

Experimental

Materials

The cellulose fiber obtained from bleached softwood pulp was obtained from Shandong Sun Holdings Group, China. TEMPO (purity ≥98 %) was supplied by Sigma-Aldrich (St. Louis, MO, USA). Sodium hydroxide (NaOH, purity ≥97 %) and sodium bromide (NaBr, purity ≥99 %) were purchased from Fu Chen (Tian Jin) Chemical Reagent Co., Ltd. Sodium hypochlorite (NaClO) solution (active chlorine content ≥7.50 %) was purchased from Guangdong Guangshi reagent Technology Co., Ltd. Ethanediol (purity ≥98%) was purchased from Sinopharm Chemical Reagent Co., Ltd. (Shanghai, China). The gelatin (~300 g Bloom) was purchased from Beijing Jinming Biotechnology Co., Ltd. The salts and other reagents were obtained from Macklin (Shanghai, China).

Preparation of DATMFC

The process began with the oxidation of softwood fibers using the TEMPO/NaBr/NaClO system, with a reaction time of 1 hour and an effective chlorine content of 1 mmol/g (cellulose).[1] Subsequently, the fibers underwent treatment using a high-speed shear device (Joyoung, China) for 2 minutes. 1.0 g resulting carboxylated microfibrillated cellulose (TMFC) were further subjected to oxidation using 1.5 g of $NaIO_4$ at 60°C for 3 hours, followed by an additional 2-minute treatment with the high-speed shear device. Finally, the sample was processed with an emulsifier (IKA, Germany) for 0 to 20 minutes to acquire dialdehyde and carboxylated microfibrilalted cellulose (DATMFC) with varying mean diameters. Similarly, dialdehyde microfibrillated cellulose (DAMFC) was prepared using the $NaIO_4$ method under the same conditions. By change mechanical cutting to mechanical grinding using a grinder (MKCA6-2J Masuko Sangyo Co., LTD, Japan) with a grinding gap of -10 μm for 50 passes at 2000rpm, $NaIO_4$-oxidized microfibrillated cellulose was further fibrillated into dialdehyde and carboxylated nanofibrilalted cellulose (DATNFC). The contents of carboxylate and aldehyde groups in DATMFC and DATNFC were the same.

Preparation of salt solutions

Various salt solutions were meticulously prepared by dissolving high-purity salts from Macklin in ultrapure water. Subsequently, the solutions were subjected to 10 minutes of sonication, resulting in the production of clear and homogeneous salt solutions.

Fabrication of TDBS hydrogels

A certain amount of gelatin was added into deionized water, and then 10 wt% of DATMFC (based on gelatin) was added into mixture in which the concentration of gelatin in mixture was maintained at 10 wt%. The mixture was stirred under 45 °C for 1 h and then poured into mold at 4 °C for gelation. Furthermore, obtained dumbbell and cylindrical shape composite hydrogels were utilized to be immersed in sodium citrate solution with different concentration for 1-120 h where the mass ratio of dumbbell and cylindrical shape composite hydrogels to sodium citrate solution was 1:21 and 1:7, respectively.

Determination of Carboxyl and Aldehyde Contents

The carboxyl and aldehyde group content of DATMFC were determined by conductometric titration and hydroxylamine hydrochloride titration, respectively.[2, 3] Here, 0.3 and 0.4 g of samples were used to determine the content of carboxyl and dialdehyde groups, respectively. The carboxyl and aldehyde groups were calculated by equation (1) and (2):

$$\text{Carboxyl content} = (C_{NaOH} \times V_{NaOH})/Ws \text{ (mmol/g)} \quad (1)$$

where C_{NaOH} means the concentration of titrant (mol/L), V_{NaOH} is the consumed volume of NaOH at the equivalence point (mL), and Ws is dried weight of samples utilized for titration.

$$AC = CV/m \text{ (mmol/g)} \quad (2)$$

where AC means the content of the aldehyde groups of DATMFC (mmol/g); C and V are the normality of NaOH (0.05 mol/L) and the consumed volume of NaOH solution, respectively.

Water loss

The water loss of composite hydrogels was determined when they were air-dried at 26 °C from 0 to 168 h. The water loss of TDBS hydrogels were calculated by equation

(3).

$$\text{Water loss}=(W_0-W_t)/W_0\times100\% \quad (3)$$

where W_0 is the initial mass of the hydrogels, W_t is the mass of the hydrogels after being placed for a certain time.

Water content test:

Water content of hydrogels after being immersed in 1.5 M sodium citrate solution for different times was recorded when they were air-dried at 105 °C for 4 h. The calculating equation is as follows:

$$\text{Water content}=(M_0-M)/M_0\times100\% \quad (4)$$

where M_0 is the initial mass of the hydrogels before immersion treatment, M is the mass of the dried hydrogels.

Nonfreezing and degradability

The nonfreezing properties of TDBS hydrogels were evaluated as follows: The ionic conductivity of 1.5GDIH-72-based sensors was assessed at -60 and -20 °C using electrochemical impedance spectroscopy (EIS). The 1.5GDIH-72-based sensors were treated at -60-0 °C, and subsequently, the samples were stored in a foam box with ice bags to mitigate the melting of ice crystals, which was evaluated through tensile tests. The 1.5GDIH-72-based strain sensors were fixed on the forefinger to detect the sensing properties of the sensor at -20, -4 and 0 °C separately.

The biodegradability of obtain composite hydrogels was explored through observing the morphological changes after being buried in soil for a few days.[4, 5]

Mechanical properties tests

The tensile strength of dumbbell shape composite hydrogels was conducted by a tensile machine (INSTRON 5565, 5000 N) where the clamp span and stretching rate were 26 mm and 10 mm/min, respectively, and then cyclic tensile test of composite hydrogels was performed after 3 pre-cycles at the strain of 30%. The thickness and gauge width of hydrogels treated by different salt solutions were measured with a caliper. Similarly, the compressive and cyclic compressive tests of cylindrical shape composite hydrogels were carried out via INSTRON 5565 at the rate of 10 mm/min, and the distance between two discs was 19 mm. Before cycling tests, a layer of silicone

oil was coated on the surface of the hydrogel to alleviate water loss.

Obtained hydrogels were designed as rectangular samples (30.0 × 15.0 × 0.8 mm^3) for shear test using INSTRON 5565, and the mass ratio between composite hydrogels and salt solutions was 1:21. The strain rate and initial clamp span were 10 mm/min and 2 mm, respectively. A 6-mm-long notch was made from the middle of the long edge towards the center of the hydrogels, and then the notched and unnotched hydrogels were loaded in pairs to acquire the fracture energy value. The fracture energy was calculated according to the following equation:[6, 7]

$$\Gamma = H\int_0^{\varepsilon_c} \sigma d\varepsilon \quad (5)$$

where H is the initial clamp span, ε_c is the critical strain of unstable propagation of crack which is from the strain at maximum stress of notched samples, and σ is the tensile stress.

Molecular dynamics simulation (MDS)

MDS were performed to study the molecular structure.[4, 5] Our simulation calculation was conducted on four structures with an integration time-step of 1 fs. Periodic boundary conditions were applied in the *x*- and *y*-dimensions. The box size of the samples was 4.1 × 4.1 × 4.1 nm^3. First, the conjugate gradient algorithm and energy minimization were performed to obtain a stable structure. Condensed-phased Optimized Molecular Potential for Atomistic Simulation Studies force field was also used to optimize these structures in the Materials studio with forcite Module. Each sample was then equilibrated under the NPT ensemble at a constant temperature of 300 K to achieve an equilibrium state with zero pressure for 10 ns. The equilibration molecular systems of the pure separation membrane could be obtained. Furthermore, a potential cutoff radius of 2.25 nm is applied in the calculation of the non-bonded interaction. And the PPPM has been used to describe the electrostatic. The Andersen feedback thermostat and Berendsen barostat algorithm are applied in the system with temperature and pressure conversion. The interaction energy can be used to measure the intensity of the interaction between molecules.

Ionic conductivity

The samples (25 × 15 × 1 mm^3) were sandwiched by copper tapes, and then measured by electrochemical impedance spectroscopy (ESI) depended on electrochemical workstation (CHI660E, Shanghai) where the frequency ranged from 0.1 Hz to 1 MHz. The conductivity of samples was calculated by the following equation:

$$\rho - 1 = L/(s \times R) = L/(s \times Z') \quad (6)$$

where ρ is the resistivity of samples, L is the effective length of ionic transport, s means the effective contact area between hydrogels and cooper tapes, R means the resistance of samples, and Z' is the real part of impedance for hydrogels.

Sensing application as strain sensors

The sensing sensitivity (GF and S) was obtained from the slope of relative resistance change-tensile strain (pressure) line after linear fitting.[8–10] The conductors from dumbbell composite hydrogels (25 × 15 × 1 mm^3) were utilized to fabricate strain sensors after being encapsulated by 3M VHB tapes. Herein, the voltage of all electrochemical tests was 4 V. Wireless Bluetooth transmission test of composite hydrogels (25 × 15 × 1 mm^3) was performed on through a self-assembled Bluetooth system. The only participant for the real-life test for hydrogel-based sensors was the author (H. C. F) of this article, who took part following informed consent. Ethical approval was not required for this work. Before sensing sensitivity tests, a layer of silicone oil was coated on the surface of the hydrogel to alleviate water loss.

General Characterization

FT-IR spectra of polymers and TDBS hydrogels were conducted by FT-IR spectrometer (VERTEX 33, Bruker, USA). Morphology of DATMFC and structure of TDBS hydrogels was characterized by FE-SEM (Zeiss, Germany). The mean diameter of DATMFC was counted from FE-SEM images via nanomeasure software 1.2. The thermal stability of TDBS hydrogels was carried out by a TA Q500 analyzer (USA). The EDS images of the hydrogel were obtained by FE-SEM. The 2D-WAXS test of the hydrogel was performed via the device of Rigaku (HomeLab, Japan) in which the x-ray wavelength (λ) is 1.5405 Å, the detector size is 100 × 100 μm, and the distance of samples to detector is 69.21812 mm. The functional groups of composite hydrogels

were recognized by X-ray photoelectron spectroscopy (Axis Ultra DLD, Kratos, England) with monochromatic Al Kα (1486.6 eV) radiation as the excitation source, and the lowest binding energy of C 1s was calibrated to 284.6 eV.

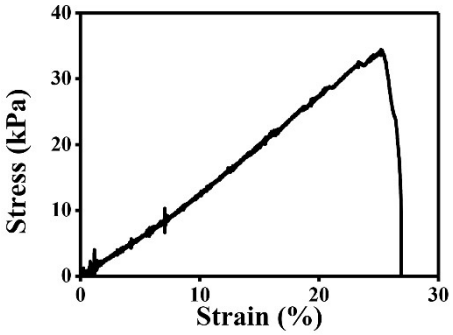

Fig. S1 Tensile curve of gelatin/DATNFC composite hydrogels.

As depicted in **Fig. S2** and **S3**, the tensile strength of composite hydrogels decreased as the mean diameter reduced from 22.92 to 17.87 μm when the addition amount of DATMFC was 10 wt%. It was evident that the tensile strength of pure gelatin hydrogels was significantly enhanced due to the presence of hydrogen bonds and imine bonds. Among all DATMFC-enhanced composite hydrogels, the hydrogel treated for 5 minutes exhibited the most excellent tensile strength (41.2 kPa). Consequently, DATMFC (5 min) was determined as the final crosslinking agent.

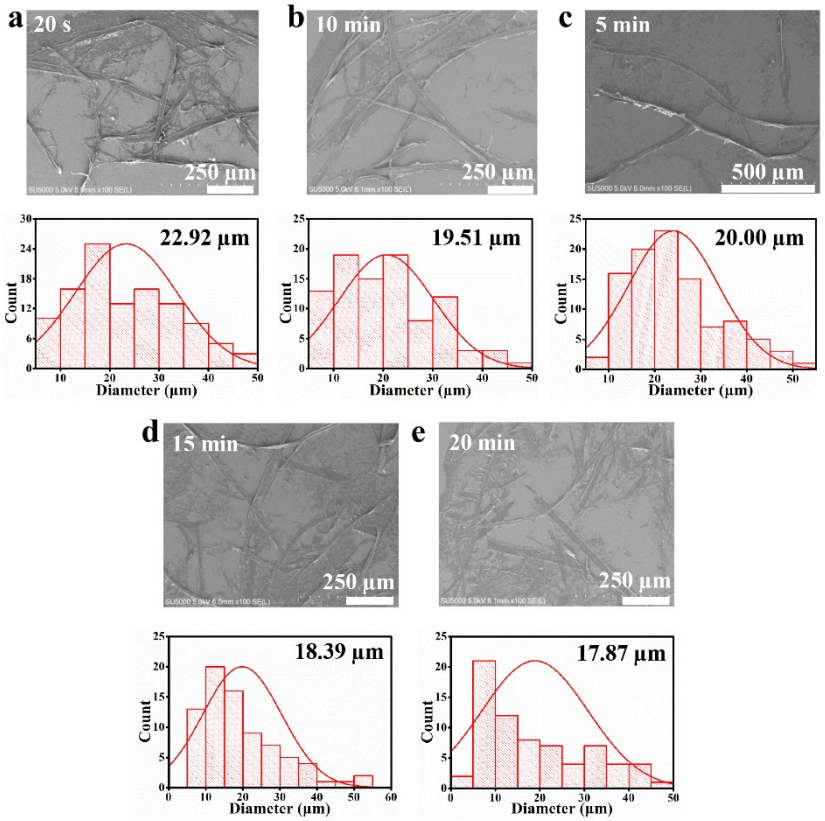

Fig. S2 Morphology and mean diameter of DATMFC with the cutting time increasing from 20 s to 20 min.

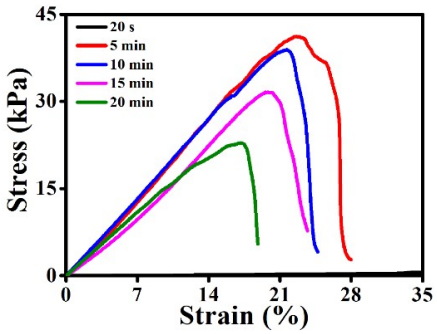

Fig. S3 Tensile curves of gelatin/DATMFC composite hydrogels.

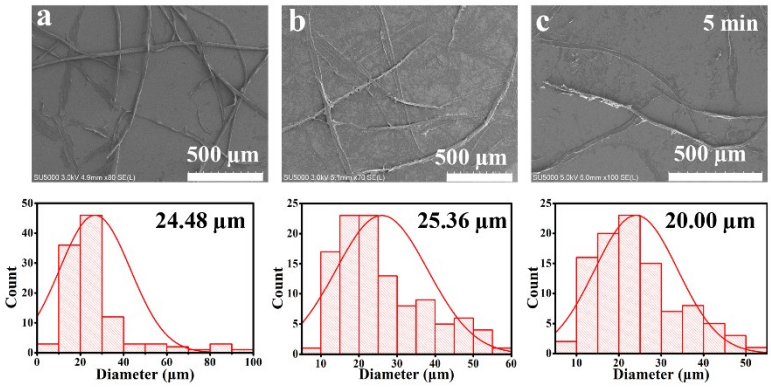

Fig. S4 Morphology and mean diameter of (a) dialdehyde cellulose and (b) carboxylated cellulose.

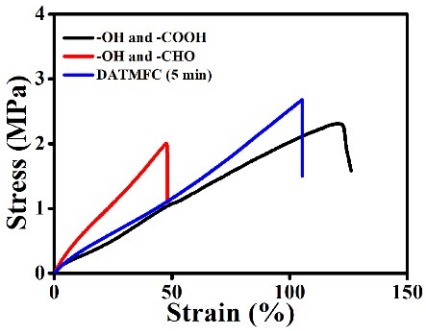

Fig. S5 Tensile curves of different cellulose enhanced composite hydrogels treated by 1.0 M sodium citrate solution for 72 h.

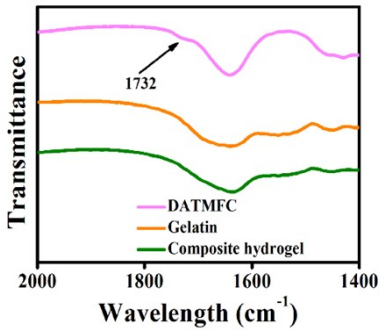

Fig. S6 FT-IR spectra of DATMFC, gelatin and gelatin/DATMFC composite hydrogels.

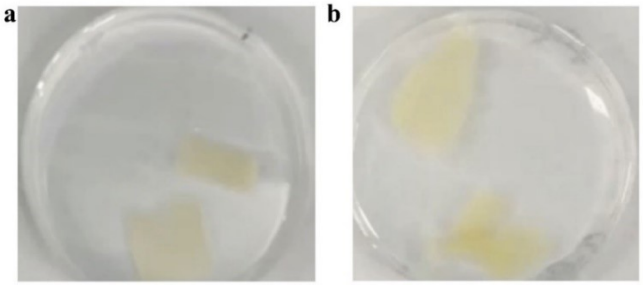

Fig. S7 Optical images of the hydrogel treated by 1.0 M (a) NaCl solution and (b) $NaHSO_4$ solution for 24 h.

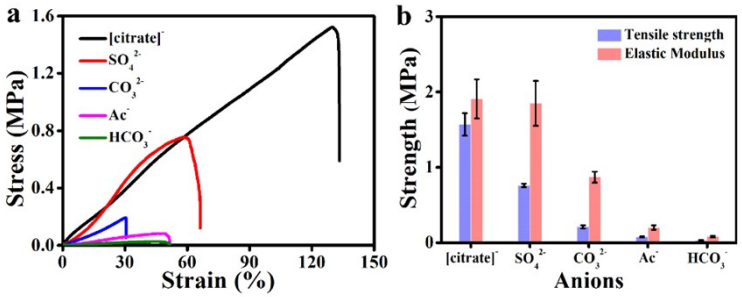

Fig. S8 Mechanical properties of TDBS hydrogels treated by different sodium salt solutions (1 M) for 24 h.

As listed in **Fig. S9a-c**, the tensile strength of TDBS hydrogels exhibited an upward trend with the increasing of sodium acetate, sodium carbonate and sodium citrate solution concentration. The tensile strength of TDBS hydrogels was improved when the sodium sulfate concentration was lower than 2.0 M (**Fig. S9d**). It was apparent that the effect of sodium citrate on hydrogen strength was best among all sodium salt solutions.

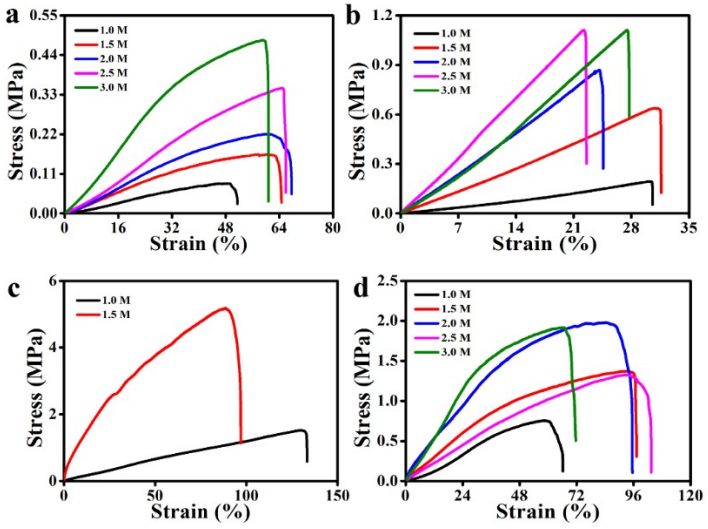

Fig. S9 Tensile curves of TDBS hydrogels treated by different concentration of (a) sodium acetate, (b) sodium carbonate, (c) sodium citrate and (d) sodium sulfate solutions for 24 h.

As presented in **Fig. S10**, the enhancement of mixed sodium salts on mechanical performance was much lower than that of single sodium salts. The results in **Fig. S10** and **S9** showed that the single sodium citrate sodium was most suitable for strengthening the mechanical strength of TDBS hydrogels.

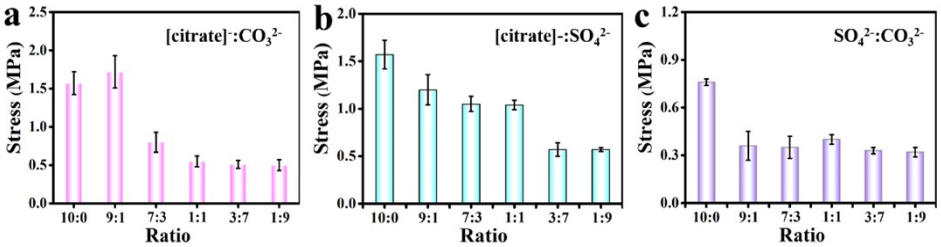

Fig. S10 Tensile curves of TDBS hydrogels treated by mixed sodium salt solution (1 M) for 24 h.

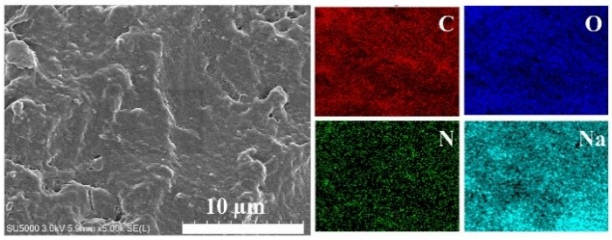

Fig. S11 EDS images of 1.5GDIH-72.

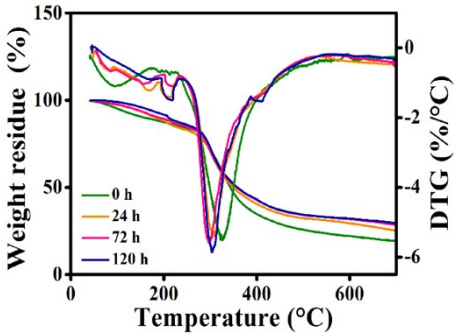

Fig. S12 Thermal stability of TDBS hydrogels treated by 1.5 M sodium citrate solution.

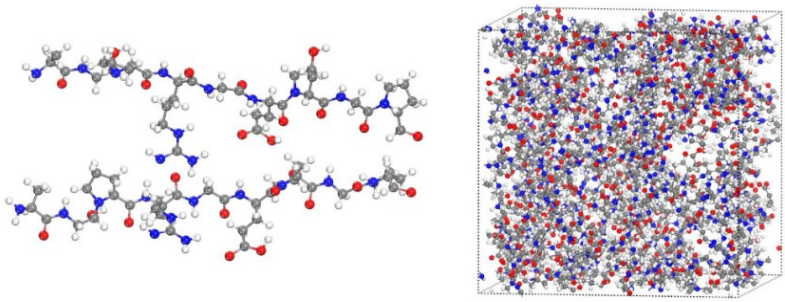

Fig. S13 Molecular structure model of G vs G.

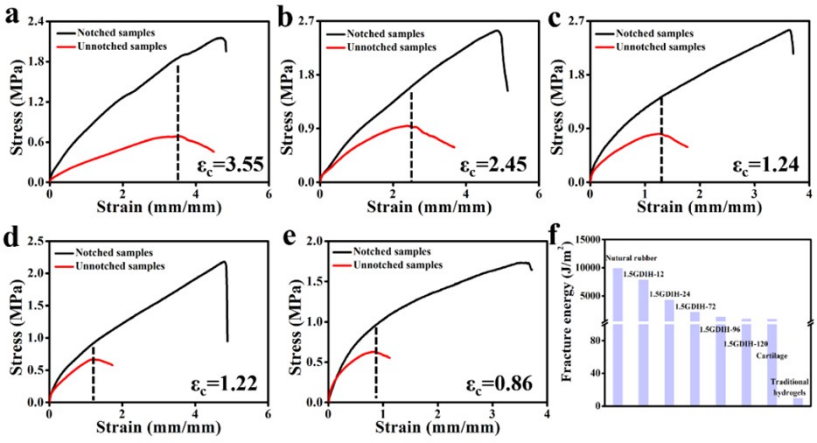

Fig. S14 Tensile curves of notched and unnotched (a) 1.5GDIH-12, (b) 1.5GDIH-24, (c) 1.5GDIH-72, (d) 1.5GDIH-96 and (e) 1.5GDIH-120. 'ε_c' represents the tensile strain. (f) Comparison of fracture energy(Γ) between the TDBS hydrogels, traditional hydrogels and cartilage.

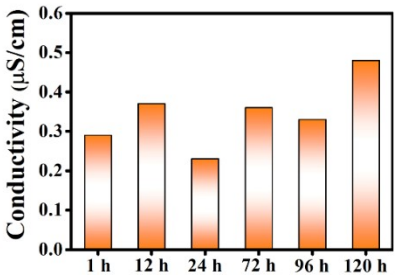

Fig. S15 Ionic conductivity of TDBS hydrogels treated by 1.5 M sodium citrate solution at 22 °C.

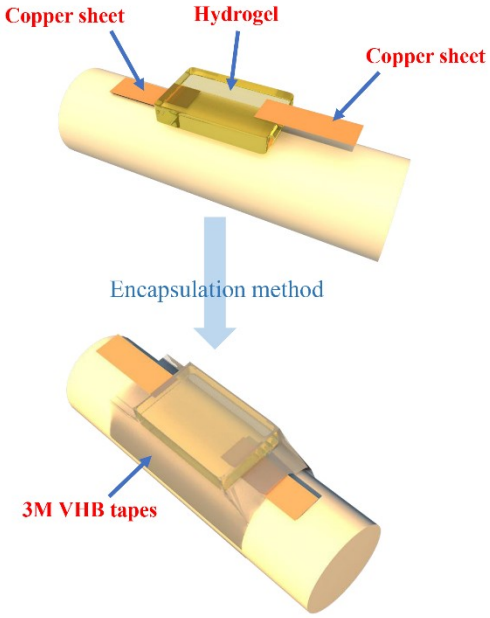

Fig. S16 Schematic illustration of the encapsulation method of hydrogel-based flexible strain sensors.

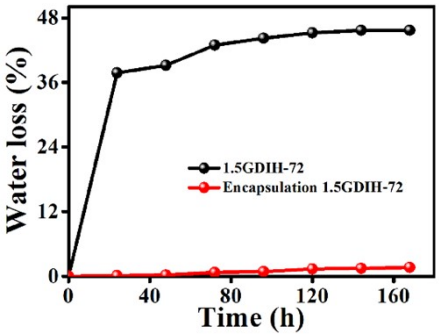

Fig. S17 Water loss of 1.5GDIH-72 and encapsulated 1.5GDIH-72 at 26 °C.

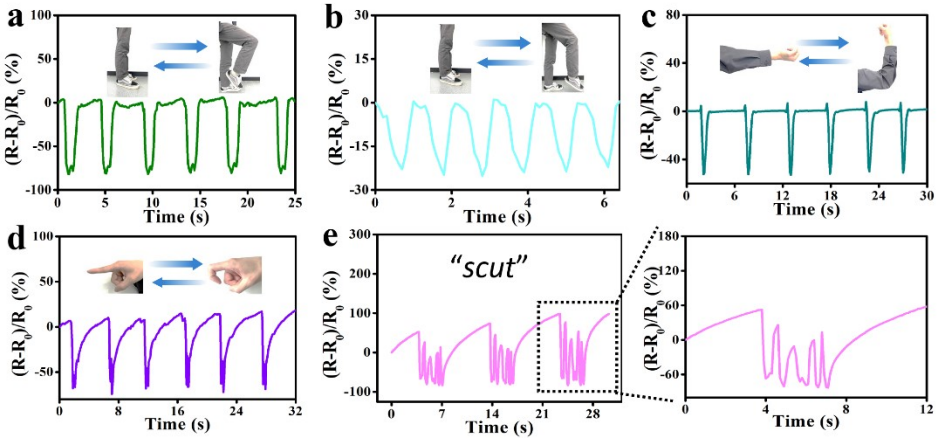

Fig. S18 Recorded relative resistance changes of the strain for (a, b) knee, (c) elbow and (d) forefinger bending, respectively. (e) Relative resistance changes of "scut" written in the same handwriting.

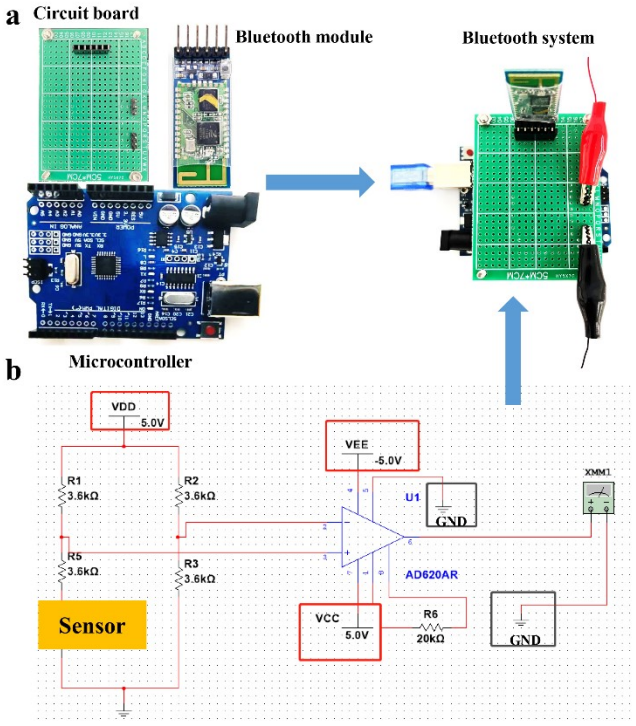

Fig. S19 (a) The demonstration of wireless sensor system and (b) integrated circuit diagram.

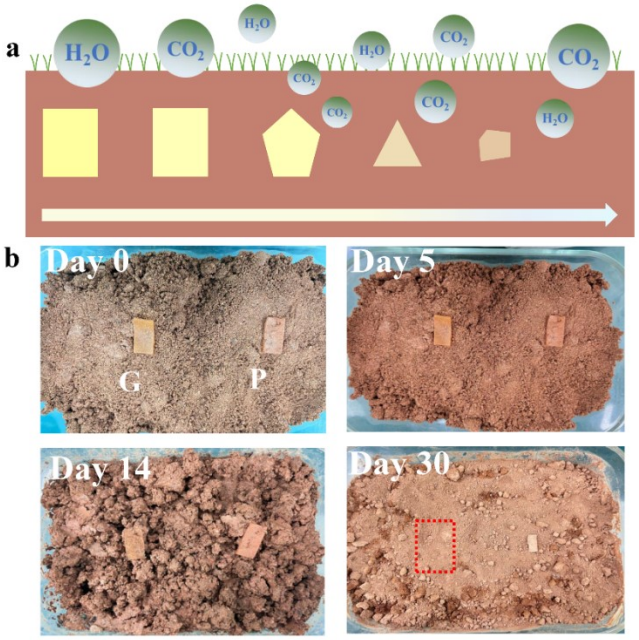

Fig. S20 (a) Schematic diagram of biodegradability process and (b) biodegradability comparison of gelatin-based TDBS hydrogels (G) and PAAm hydrogels (P).

Table S1. -COOH and -CHO group content of different cellulose.

Cellulose	COOH	-CHO
Cellulose with single -COOH	0.38	/
Cellulose with single -CHO	/	1.26
Cellulose with low content of -COOH and -CHO (DATMFC)	0.38	1.74

Table S2. The $T_{10\%}$, $T_{50\%}$ and T_{max} of composite hydrogels where $T_{10\%}$ and $T_{50\%}$ represented the temperature at 10 and 50% of mass loss, respectively, and T_{max} is the temperature at maximum degradation rate.

Immersion time	$T_{10\%}$/°C	$T_{50\%}$/°C	T_{max}/°C
0	159.3	342.8	325.8
24	182.7	349.2	306.6
72	190.8	356.8	303.9
120	210.1	358.1	298.5

Table S3. Water content of composite hydrogels after being immersed in 1.5 M sodium citrate solution for different times.

Immersion time (h)	0	24	48	72	96
Water content (%)	89.0±0.5	47.6±1.1	47.4±0.5	44.1±0.2	43.6±0.2

Video S1. Movie showing on-line monitoring from natural bending of forefinger wirelessly displayed on a mobile phone in a real-time manner. Movie viewable at https://doi.org/10.1039/d3mh02008h

References

[1] H. C. Fu, B. Wang, J. P. Li, J. Xu, J. Li, J. S. Zeng, W. H. Gao and K. F. Chen, *Mater. Horiz.*, 2022, **9**, 1412-1421.

[2] J. P. Li, L. Kang, B. Wang, K. F. Chen, X. J. Tian, Z. Ge, J. S. Zeng, J, Xu and W. H. Gao, *ACS Sustainable Chem. Eng.*, 2019, **7**, 1146-1158.

[3] P. F. Li, J. S. Zeng, B. Wang, Z. Cheng, J. Xu, W. H. Gao and K. F. Chen, *Carbohydr. Polym.*, 2020, **247**, 116721.

[4] X. H. Zhang, P. F. Li, J. S. Zeng, J. P. Li, B. Wang, W. H. Gao J. Xu and K. F. Chen, Ch*em. Eng. J.*, 2023, **465**, 143017.

[5] G. W. Zhou, H. S. Zhang, Z. P. Su, X. Q. Zhang, H. N. Zhou, L. Yu, C. J. Chen and X. H. Wang, *Adv. Mater.*, 2023, **35**, 2301398.

[6] J.-Y. Sun, X. H. Zhao, W. R. K. Illeperuma, O. Chaudhuri, K. H. Oh, D. J. Mooney, J. J. Vlassak and Z. G. Suo, *Nature*, 2012, **489**, 133-136.

[7] M. T. Hua, S. W. Wu, Y. F. Ma, Y. S. Zhao, Z. L. Chen, I. Frenkel, J. Strzalka, H. Zhou, X. Y. Zhu and X. M. He, *Nature*, 2021, **590**, 594-599.

[8] R. Cheng, J. S. Zeng, B. Wang, J. P. Li, Z. Cheng, J. Xu, W. H. Gao and K. F. Chen*, Chem. Eng. J.*, 2021, **424**, 130565.

[9] H. J. Ding, Z. X. Wu, H. Wang, Z. J. Zhou, Y. M. Wei, K. Tao, X. Xie and J. Wu, *Mater. Horiz.*, 2022, **9**, 1935-1946.

[10] H. L. Huang, L. Han, J. F. Li, X. B Fu, Y. L. Wang, Z. L. Yang, X. T. Xu, L. K. Pan and M. Xu, *J. Mater. Chem. A*, 2020, **8**, 10291-10300.